



Identification of miRNA Associated with Reduced Survival after Whole-Thorax Lung Irradiation in Non-Human Primates

Authors: Rogers, Claude J., Kyubwa, Espoir M., Lukaszewicz, Agnes I., Yamada-Hanff, Jason, Starbird, Mark A., et al.

Source: Radiation Research, 196(5) : 510-522

Published By: Radiation Research Society

URL: <https://doi.org/10.1667/RADE-20-00031.1>

BioOne Complete (complete.BioOne.org) is a full-text database of 200 subscribed and open-access titles in the biological, ecological, and environmental sciences published by nonprofit societies, associations, museums, institutions, and presses.

Your use of this PDF, the BioOne Complete website, and all posted and associated content indicates your acceptance of BioOne's Terms of Use, available at www.bioone.org/terms-of-use.

Usage of BioOne Complete content is strictly limited to personal, educational, and non - commercial use. Commercial inquiries or rights and permissions requests should be directed to the individual publisher as copyright holder.

BioOne sees sustainable scholarly publishing as an inherently collaborative enterprise connecting authors, nonprofit publishers, academic institutions, research libraries, and research funders in the common goal of maximizing access to critical research.

Identification of miRNA Associated with Reduced Survival after Whole-Thorax Lung Irradiation in Non-Human Primates

Claude J. Rogers,^a Espoir M. Kyubwa,^a Agnes I. Lukaszewicz,^a Jason Yamada-Hanff,^a Mark A. Starbird,^a Thomas A. Miller,^a Asa A. Phelps,^a Seth Wallack,^b Saikanth Mahendra,^c Karla Thrall^d and Naresh Menon^{a,1}

^a ChromoLogic LLC, Monrovia, California 91016; ^b Veterinary Imaging Center of San Diego, San Diego, California 92111; ^c Northwest Medical Physics Center, Lynnwood, Washington 98036; and ^d Altasciences Preclinical Seattle LLC, Everett, Washington 98203

Rogers, C. J., Kyubwa, E. M., Lukaszewicz, A. I., Yamada-Hanff, J., Starbird, M. A., Miller, T. A., Phelps, A. A., Wallack, S., Mahendra, S., Thrall, K. and Menon, N. Identification of miRNA Associated with Reduced Survival after Whole-Thorax Lung Irradiation In Non-Human Primates. *Radiat. Res.* 196, 510–522 (2021).

Thoracic exposure to ionizing radiation can lead to delayed injuries to the heart and lung that are serious and even life-threatening. These injuries are difficult to predict since they manifest over many weeks and months. To identify non-invasive, tissue-specific biomarkers for the early detection of late radiation injury, circulating microRNA (miRNA) levels were measured in non-human primates (NHP, *Macaca mulatta*) that received a single exposure of whole-thorax lung irradiation (WTLI) at a dose likely to result in 20% or 75% mortality within 180 days (9.8 or 10.7 Gy). Animals were observed for 270 days after WTLI. Approximately 58% of 9.8 Gy WTLI animals (7 of 12) and 94% of 10.7 Gy WTLI animals (15 out of 16) did not survive to the primary end point. Evidence of pulmonary fibrosis/pneumonitis was observed in all animals. Animals that received 10.7 Gy WTLI experienced more severe and early-onset pneumonitis, as indicated by reduced aerated lung volume, high non-sedated respiratory rate, earlier and more frequent dexamethasone treatments, and evidence of onset of heart disease. Radiation-induced changes in the circulating miRNA profile were most prominent within the first 30 days postirradiation, before the manifestation of symptoms, and included miRNA sequences known to regulate pathways associated with pulmonary fibrosis (TGF- β /SMAD signaling) and pneumonitis/inflammation (p53 signaling). The abundance of several circulating miRNA differentially expressed at day 6 or 15, such as miR-199a-3p and miR-25-3p, correlated with statistically significant differences in survival. This study supports the hypothesis that it is feasible to use plasma miRNA profiles to identify individuals at high risk of organ-specific late radiation injury. These miRNA profiles could improve radiation oncology clinical practice and serve as biomarkers to predict who might develop late complications

Editor's note. The online version of this article (DOI: <https://doi.org/10.1667/RADE-20-00031.1>) contains supplementary information that is available to all authorized users.

¹ Address for correspondence: ChromoLogic, 1225 S Shamrock Ave., Monrovia, CA 91016; email: nmenon@chromologic.com.

in the aftermath of a radiological or nuclear (RAD-NUC) incident. © 2021 by Radiation Research Society

INTRODUCTION

Triage after a mass casualty radiation event is complex because of the diverse array of adverse responses, the non-uniformity of absorbed dose resulting from partial-body shielding by physical barriers and the lack of adequate biodosimetry. Depending on the nature of the exposure, such an incident could result in morbidity and mortality resulting from acute radiation syndrome (ARS) associated with the hematopoietic (H-ARS) or gastrointestinal (GI-ARS) system, or delayed effects of acute radiation exposure (DEARE) to the pulmonary, cardiovascular or other systems in the body. Hematopoietic or gastrointestinal ARS results in death within days to weeks postirradiation, and is characterized by the loss of organ-specific stem and progenitor cells in the bone marrow (H-ARS) and intestinal crypt cells (GI-ARS) (1). Unlike ARS, DEARE can manifest within weeks, months or years postirradiation and the severity varies with the degrees of partial-body shielding, pre-existing conditions, and a host of factors that are typical of a mass casualty radiation event that occurs where there is a diverse urban population (2). As a result, while an individual may not show any symptoms of ARS and may survive the early days from such an incident, they may be highly vulnerable to DEARE and succumb to injuries within months. Therefore, the ability to predict these adverse outcomes of acute radiation exposure before the manifestation of symptoms would allow for effective triage, especially since early therapeutic intervention can dramatically improve survival rates in the context of ARS (3–8), and perhaps late disease (4). Investigators have identified potential biomarkers of radiation exposure in blood or plasma, including proteins (9–12), mRNAs (13–18), non-coding RNA (19) and microRNAs (miRNAs) (20–26). Furthermore, because circulating miRNAs are protected from degradation in extracellular vesicles or protein

complexes that are stable at room temperature for hours to days, they are exceptionally well suited for point-of-care sample collection and processing with standard molecular testing instruments (27).

miRNAs are small (19–22 nt), non-coding nucleotides that post-transcriptionally regulate protein expression (28). Approximately 1–2% of all genes in mammals encode for miRNAs. miRNAs can be released into extracellular biofluids, such as plasma, and may participate in cell-cell and tissue-tissue communication (29). Changes in the circulating miRNA profile have been observed in pathophysiological conditions, such as cancer (30, 31), and after exposure to radiation (20–26). Since miRNAs can be tissue-specific (32, 33), the circulating miRNA profile may reflect what tissues are injured (34–37). While this field is still in its infancy, we and others have shown that total-body irradiation (TBI) drives significant alterations in circulating hematopoietic miRNA biomarkers, such as miR-150-5p, and the extent of dysregulation correlates well with the later onset of neutropenia and lymphopenia in an individual animal (21–23). We have also shown that in mice that received whole-thorax lung irradiation (WTLI) for late radiation injury to the heart and lung with shielding to prevent ARS mortality, survival of a strain susceptible to developing radiation-induced pneumonitis (C3H) (38) was associated with changes in miRNA expression associated with pro-inflammatory NF- κ B-mediated signaling pathways (miR-34a-5p, -100-5p and -150-5p) and survival of a strain that tends to develop radiation-induced fibrosis (C57Bl/6) (39) was associated with changes in expression of miRNAs associated with TGF- β /SMAD signaling (miR-34b-3p, -96-5p and -802-5p) (40).

Here, we used a WTLI model of non-human primates (NHP; *M. mulatta*) to induce late radiation injury to the heart and lung without ARS. NHPs received a single fraction of either 9.8 or 10.7 Gy WTLI and were observed for 270 days postirradiation for moderate and severe radiation-induced injuries, respectively. Changes in circulating miRNA were assessed longitudinally after WTLI. Local and systemic radiation damage was also monitored by changes in body weight, respiratory rates, hematology, computed tomography (CT) and histology. We observed major radiation-induced changes in systemic circulating miRNA profiles and found that miRNA that correlated with survival were associated with the well-known pathogenesis of late lung injury (pneumonitis and fibrosis) and cardiac fibrosis. Our results indicate that miRNA profiling may be used to predict late organ injury long before the manifestation of symptoms.

MATERIALS AND METHODS

Animals

For this study, 14 male (3.93 ± 0.18 kg body weight, 3–4 years old) and 14 female (4.05 ± 0.26 kg body weight, 3–4 years old) rhesus macaques (*Macaca mulatta*; Chinese origin) were used. All animals underwent routine quarantine and health checks before inclusion into the study as described elsewhere (41, 42). Animal housing and care was compliant with the Animal Welfare Act and recommendations set

forth in the Guide for the Care and Use of Laboratory Animals (National Research Council, 2011). All procedures were carried out in compliance with institutional policies on the Humane Care and Use of Laboratory Animals and were approved by the Institutional Animal Care and Use Committee (IACUC). Prior to inclusion into the study, all animals were acclimated to the facility for 14 days. Animals found to have abnormal baseline complete blood count (CBC), evidence of lung disease, injury or poor health were excluded from the study. During the acclimation period, baseline ungated thoracic CT scan was acquired per CT scan acquisition procedure.

Group Assignments and Irradiation

Animals were randomly assigned to receive 9.8 Gy ($LD_{20/180}$; 6 males, 6 females) or 10.7 Gy ($LD_{75/180}$; 8 males, 8 females) WTLI at a dose rate of 0.60 ± 0.10 Gy min^{-1} . Prior to WTLI, animals were administered antiemetic (ondansetron HCL, 1.9 mg kg^{-1}) and anesthetized with Ketamine/Xylazine. Sedated animals were restrained on the linear accelerator (LINAC) couch. Radiation was delivered using a 6-MV photon source LINAC (Varian CLINAC 21EX; Varian Medical Systems Inc., Palo Alto, CA) in an anterior-posterior (AP) and posterior-anterior (PA) technique with approximately 50% dose contribution from both the AP and PA beams (41, 43).

Clinical Observations

After irradiation, cage-side clinical observations were performed twice daily. Observations included non-sedated respiratory rate (NSRR), activity, stool consistency, vomiting and posture. In addition to clinical observations, each animal was weighed twice during the acclimation period and weekly postirradiation. Rectal pulse oximetry was performed twice weekly postirradiation on non-sedated animals. Blood samples for hematology and serum chemistry were collected by venipuncture in EDTA-containing tubes at day -2, and every 3 days postirradiation through days 30, 40, 50 and 60, and then every 30 ± 3 days thereafter. Blood samples for miRNA analysis were collected before irradiation, and at days 6, 12, 15, 30, 60 and 90 postirradiation.

Dexamethasone Supportive Therapy for Tachypnea/Pneumonitis

Animals that developed tachypnea and respiratory distress indicative of pneumonitis, defined as NSRR >80 breaths/min, received medical supportive therapy (dexamethasone) following a scheduled taper described below (41, 44). In the schedule, the first course of treatment was administered intramuscularly (IM) using the following regimen: 1.0 mg kg^{-1} twice daily (BID) on the first day of treatment; 0.5 mg kg^{-1} BID for 3 days; 0.5 mg kg^{-1} once daily (SID) for 3 days; 0.5 mg kg^{-1} every other day for three doses. For animals that developed respiratory distress within 7 days of stopping the first course of treatment, the second course of treatment was as follows: 1.0 mg kg^{-1} SID on the first day of treatment; 0.5 mg kg^{-1} SID for 4 days; 0.5 mg kg^{-1} every other day for 10 doses. For animals that developed respiratory distress outside 7 days of stopping the first course of treatment, the second course of treatment was as follows: 1.0 mg kg^{-1} BID on the first day of treatment; 0.5 mg kg^{-1} BID for 3 days; 0.5 mg kg^{-1} SID for 3 days; 0.5 mg kg^{-1} every other day for 10 doses. For animals that completed two courses of dexamethasone treatment and required additional medical supports, a veterinary consultation was obtained and treatment with dexamethasone was conducted by veterinary recommendation. Animals with repeated episodes of respiratory distress and non-responsive to treatment met criteria for euthanasia. Onset of radiation-induced pneumonitis was measured by the timing to first dexamethasone administration, displayed as mean \pm standard error of the mean.

Euthanasia

Euthanasia criteria included any of the single criterion or two or more of the combination criteria. Single criterion included observation

of: 1. respiratory distress (e.g., open mouth breathing, cyanotic appearance, labored breathing, respiratory rate ≥ 80 breaths/min) and non-responsive to dexamethasone treatment; 2. inactivity (e.g., recumbent in the cage for at least 15 min, or non-responsive to touch); 3. uncontrolled hemorrhage from any orifice; 4. unrelieved pain or distress after administration of two consecutive increased doses of buprenorphine (0.02 mg/kg IM BID); or 5. severe dehydration. Combination criterion included two or more observations of: 1. hyperthermia (rectal temperature $\geq 41^\circ\text{C}$); 2. hypothermia (rectal temperature $\leq 35^\circ\text{C}$); 3. weight loss ($\geq 25\%$ of baseline) for two consecutive days; 4. severe injury or condition (e.g., minor bone fracture, progressive tissue necrosis, non-healing wound); 5. complete anorexia for 48 h. Surviving animals were euthanized at day 270 postirradiation. Animals that met the criteria for euthanasia were sedated and blood was collected for hematology, serum chemistry and biomarker discovery. If possible, CT scan was acquired prior to blood collection. At euthanasia, animals were weighed and euthanized by intravenous injection of a pentobarbital overdose, followed by necropsy.

Computed Tomography Scans and Image Analysis

To evaluate the severity of the radiation-induced lung injury, serial CT scans were acquired every 30 ± 3 days postirradiation until end point (day 270) or until IACUC criteria for euthanasia were met. Non-contrast CT scans were acquired with the animal sedated and positioned supine, head-first into the scanner, arms overhead and restrained on the table. A spiral CT scan (SOMATOM Scope, Siemens Medical Solutions USA, Inc., Malvern, PA) with slice thickness of 1.5 mm was acquired with a lung window reconstruction using 80-kV potential, 111 mAs, 1.0 rotation time, 0.4 pitch level and B70s kernel. CT scans were read and analyzed by an experienced veterinarian radiologist on the ClearCanvas Workstation (version 2.0.12729.37986 SPI; Synaptive Medical, Toronto, Canada). To calculate lung volumes and quantify extent of lung injury, the radiologist performed a three-dimensional (3D) volumetric reconstruction of the thoracic CT radiographs with 3D Slicer (version 4.7.0-2017-08-12 r26243; <http://www.slicer.org>) using a semiautomated radiodensity (Hounsfield units, HUs) thresholding (41, 43): aerated lung volume (-880 to -220); active pneumonitis and fibrosis (-300 to $+88$). Portions of lung boundaries that were falsely included in the initial lung boundaries were manually excluded and portions of the lung boundaries that were falsely excluded were manually included. Pleural effusions and atelectasis were separately identified manually. Data are presented as aerated lung volumes, excluding normal soft tissue, vasculature and areas of pneumonitis/fibrosis from the volume calculation.

Histopathology

To assess the degree of tissue damage, lung and heart tissues were collected, trimmed, formalin-fixed, paraffin-embedded, sectioned, and stained with hematoxylin and eosin (H&E) or Masson's Trichrome (MT). Sections of the right and left cranial and caudal lung lobes, the right medial lung lobe, and longitudinal sections of the right and left ventricle and atria and the septum of the heart, through the middle of these structures, were taken. Slides were then microscopically examined and scored by an experienced board-certified veterinarian pathologist for inflammatory cell infiltrates and collagen deposition in irradiated tissue. For each histological alteration, a severity score from 0 to 4 was assigned, corresponding to undiscernible, minimal, mild, moderate and marked, respectively (45).

miRNA Analysis by Next-Generation Sequencing

Plasma was checked for excess hemolysis using UV-vis spectroscopy, and samples with an absorbance value greater than 1.2 absorbance units at 415 nm, corresponding to 0.3% hemolysis (46), were excluded from the study. Circulating plasma miRNA was

isolated from 100 ml of plasma using the miRNEasy Serum/Plasma Advanced Kit (QIAGEN®, Valencia, CA). Libraries for sequencing were prepared using the QIAseq miRNA Library Kit (QIAGEN), with 5.8 ml of miRNA extracts as input, a 1:10 dilution of the 3'-adaptor, a 1:5 dilution of the 5'-adaptor, a 1:10 dilution of the RT primer and 22 amplification cycles. The concentrations of the prepared libraries were determined via Bioanalyzer analysis (2100 Electrophoresis Bioanalyzer; Agilent Technologies Inc., Santa Clara, CA). Libraries with an adaptor dimer peak (~ 160 nt) at least five times greater than the library peak (~ 180 nt) were not sequenced. miRNA counts for 2-nM samples were determined via next-generation sequencing (NextSeq 550; Illumina®, San Diego, CA) using 76 read cycles. Demultiplexing, trimming (read lengths between 18–40 bp, 5'-end base quality ≥ 30 , read score ≥ 20 , and 3'-end adaptor sequence to trim of AACTGTAGGCACCATCAAT), and miRNA alignment (using "Homo sapiens/hg19" as the species) was performed using BaseSpace (Illumina), using the Small RNA v1.0.1, FASTQ Toolkit version 2.2.0, and FASTQ Generation version 1.0.0. Sequencing runs with less than 100,000 miRNA reads were rejected.

Data Analysis

Raw sequencing counts were normalized by total library size to obtain the reads for a given sequence-per-million total reads (RPM), then by quantile normalization of the \log_2 RPM. Differential expression analysis was performed in R version 3.4.3 using normalized counts, using the limma and voom software packages (version 3.28.10) (47). KEGG pathways associated with differentially expressed miRNA were identified using mirPath version 3 software (48). Kaplan-Meier survival curves were compared using the log-rank test (Mantel-Cox) (49), and uncertainties (95% confidence intervals) estimated according to Greenwood (50). Blood count data were compared over time using an analysis of variance (ANOVA) model, and *P* values were obtained by comparing postirradiation values to preirradiation values using Dunnett's method. Statistical differences between prevalence score distributions were quantified using the Mann-Whitney U test.

RESULTS

Hematology and Mortality after WTLI

NHPs experienced a drop in total WBC (1.5-fold, $P < 0.001$) and lymphocyte (2-fold, $P < 0.002$) counts within the first few days after WTLI (Fig. 1). Total WBC and lymphocyte counts returned to preirradiation levels one month after WTLI. Neutrophil counts increased starting at one month after WTLI and remained elevated until at least month 4 (2–4-fold, $P < 0.0005$). Animals that received 10.7 Gy WTLI showed a sharper increase in neutrophil counts than animals that received 9.8 Gy in one and two months after irradiation (1.3–2.4-fold, $P < 0.005$). Platelet counts remained stable at preirradiation levels in animals receiving 9.8 or 10.7 Gy WTLI.

Approximately 58% of 9.8 Gy WTLI animals (7 of 12) and 94% of 10.7 Gy WTLI animals (15 of 16) died due to late radiation injury. Overall survival rates differed for animals that received 9.8 or 10.7 Gy (log-rank $P = 0.0001$). Fifty percent of the 9.8 Gy WTLI animals survived 120–180 days, with no significant differences between genders (Fig. 2A). Animals that received 10.7 Gy had higher rates of mortality (log-rank $P = 0.0001$), with 50% of the animals surviving 60–100 days and males having reduced survival

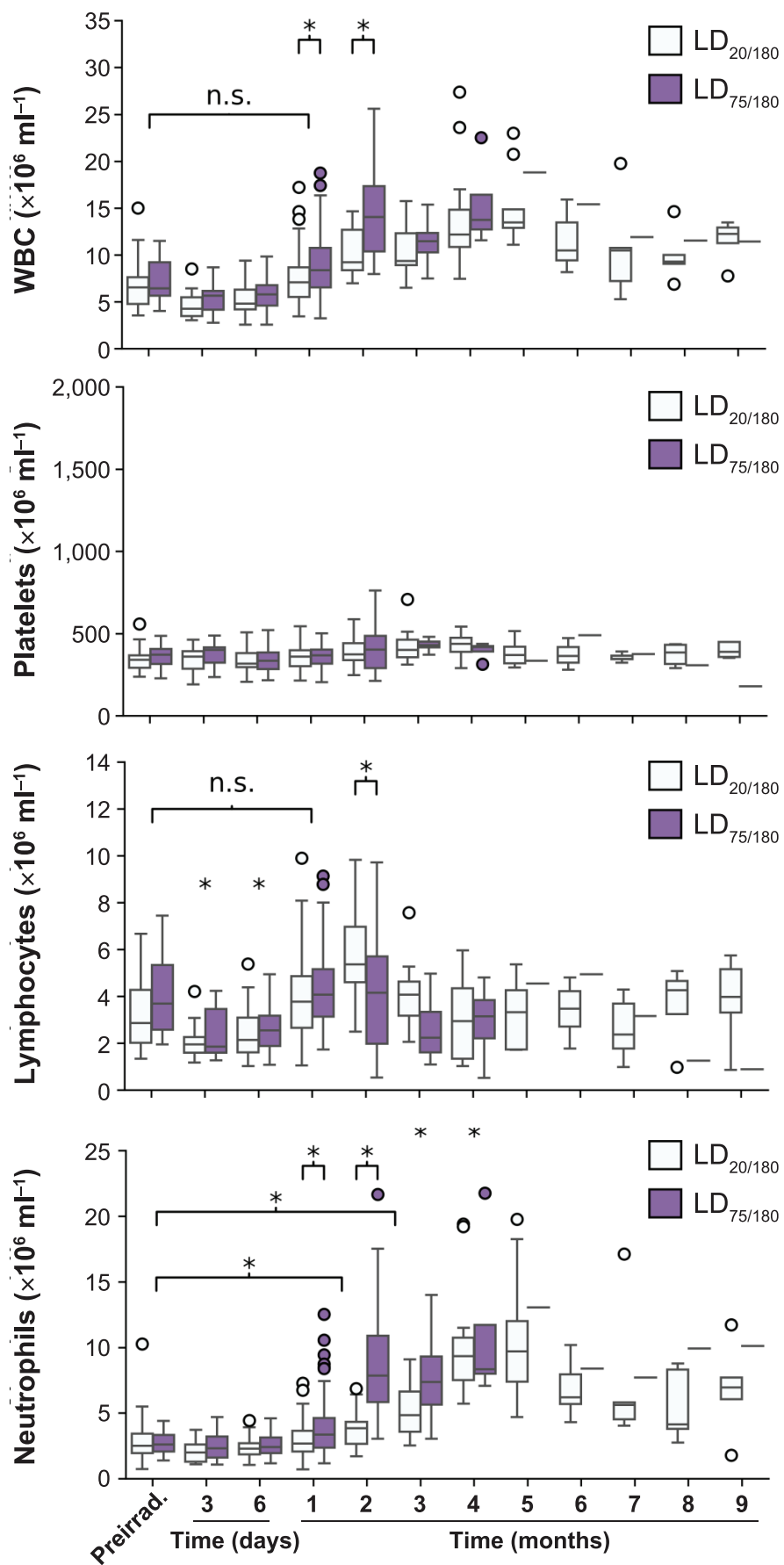


TABLE 1

Dose/gender	Average first day of dexamethasone administration for all treatment courses					
	1st	2nd	3rd	4th	5th	6th
9.8 Gy	91 ± 3	110 ± 4	136 ± 7	163 ± 11	196 ± 35	209 ± 48
Females	94 ± 4	115 ± 6	143 ± 9	168 ± 16	204 ± 59	161 ^a
Males	87 ± 5	105 ± 5	127 ± 8	156 ± 20	180 ^a	256 ^a
10.7 Gy	55 ± 5	83 ± 9	108 ± 16	153 ^a	174 ^a	-
Females	63 ± 8	88 ± 10	122 ± 14	153 ^a	174 ^a	-
Males	46 ± 3	56 ^a	-	-	-	-

Notes. Data presented as mean ± standard error of the mean.

^a Single animal.

compared to females (log-rank $P = 0.009$; Fig. S1; <https://doi.org/10.1667/RADE-20-00031.1.S1>).

Respiratory Rate and Time of Onset of Clinical Pneumonitis

All animals exhibited a gradual increase in respiratory rate, beginning 40–45 days postirradiation. On average, the respiratory rate was significantly increased over preirradiation levels by 40 days after 10.7 Gy WTLI (1.4-fold, $P < 10^{-7}$) and by 80 days after 9.8 Gy WTLI (1.3-fold, $P < 0.002$; Fig. 3D). Furthermore, the average respiratory rate exceeded 80 breaths/min⁻¹ by 70 days after 10.7 Gy WTLI, compared to 120 days after 9.8 Gy WTLI (Fig. 3D). Interestingly, the average respiratory rate of 9.8 Gy WTLI animals began to decrease after peaking between days 130–140 postirradiation but did not recover to preirradiation levels (60 vs. 45 breaths/min⁻¹; $P < 10^{-5}$).

Overall, the onset of tachypnea and respiratory distress indicative of pneumonitis (NSRR > 80 breaths/min⁻¹) occurred earlier in 10.7 Gy WTLI animals than in 9.8 Gy animals (mean time to initial dexamethasone treatment of 55 days vs. 91 days; log-rank $P = 0.001$; Fig. 2B and Table 1). The onset of these symptoms, as measured by the date of first dexamethasone treatment, affected all animals and strongly correlated with survival (correlation coefficient = 0.88; Fig. 2C).

Radiologic Evidence of Fibrosis/pneumonitis

CT radiographs revealed dose-dependent increase in radiodensity, indicative of radiation-induced lung injury starting at day 60 after WTLI (Fig. 3A). At day 60 postirradiation, 10.7 Gy WTLI animals exhibited a significant decrease in aerated lung volume from preirradiation volume (29% decrease, 108 ± 33 ml vs. 151 ± 24 ml; $P < 0.0005$, Fig. 3B), compared to 9.8 Gy WTLI

animals (9% decrease, 149 ± 26 ml vs. 163 ± 26 ml, $P = 0.18$). By day 90 postirradiation, both the 9.8 Gy and 10.7 Gy WTLI groups exhibited significant decrease in aerated lung volume from preirradiation (33% decrease, 101 ± 26 ml vs. 151 ± 24 ml, $P < 0.005$; 17% decrease, 136 ± 19 ml vs. 163 ± 26 ml, $P < 0.01$, respectively).

Histological Evidence of Radiation-induced Lung and Cardiac Injury

Evidence of radiation-induced lung and heart injury was also characterized by histology, performed at the time of death. Histological evidence of heart injury included infiltration of mononuclear cells, myocardium degeneration and interstitial fibrosis. These effects were more prevalent in animals receiving 10.7 Gy WTLI (Mann-Whitney U test $P < 0.05$; Fig. 4). Evidence of prevalent lung injury was more frequently observed. Infiltration of macrophages and neutrophils, as well as fibrin deposits, was observed in the alveolar space. Interstitial fibrosis and mononuclear cell invasion were also observed (Fig. 4C). A statistical difference was observed between the prevalence distributions of the infiltration of neutrophils into the alveolar space and interstitial invasion of mononuclear cells (Mann-Whitney U test $P < 0.05$).

Differential Expression of Circulating miRNA

Differential expression analysis of next-generation miRNA sequencing data of circulating miRNA from plasma revealed that WTLI affects the expression of a number of sequences (Fig. 5). At 6, 15, 24 days and 1, 2 and 3 months after WTLI, the circulating miRNA profile was compared to the preirradiation profile for NHPs that received 9.8 or 10.7 Gy WTLI. For both doses, differentially expressed miRNAs (fold change > 2.25 and $P < 0.05$) were observed at all

←

FIG. 1. Blood cell counts for NHPs receiving 9.8 or 10.7 Gy whole-thorax lung irradiation (WTLI). WTLI resulted in an early drop in white blood cells (WBC) and lymphocytes that recovered by month 1 and became slightly elevated by month 2, with some dose-dependent differences. Platelets were not significantly changed. Neutrophil counts were elevated by month 1, but were more persistently elevated in animals that received 10.7 Gy WTLI. Statistically significant changes in counts compared to preirradiation levels or between the dose cohorts. * $P < 0.001$, Dunnett's test.

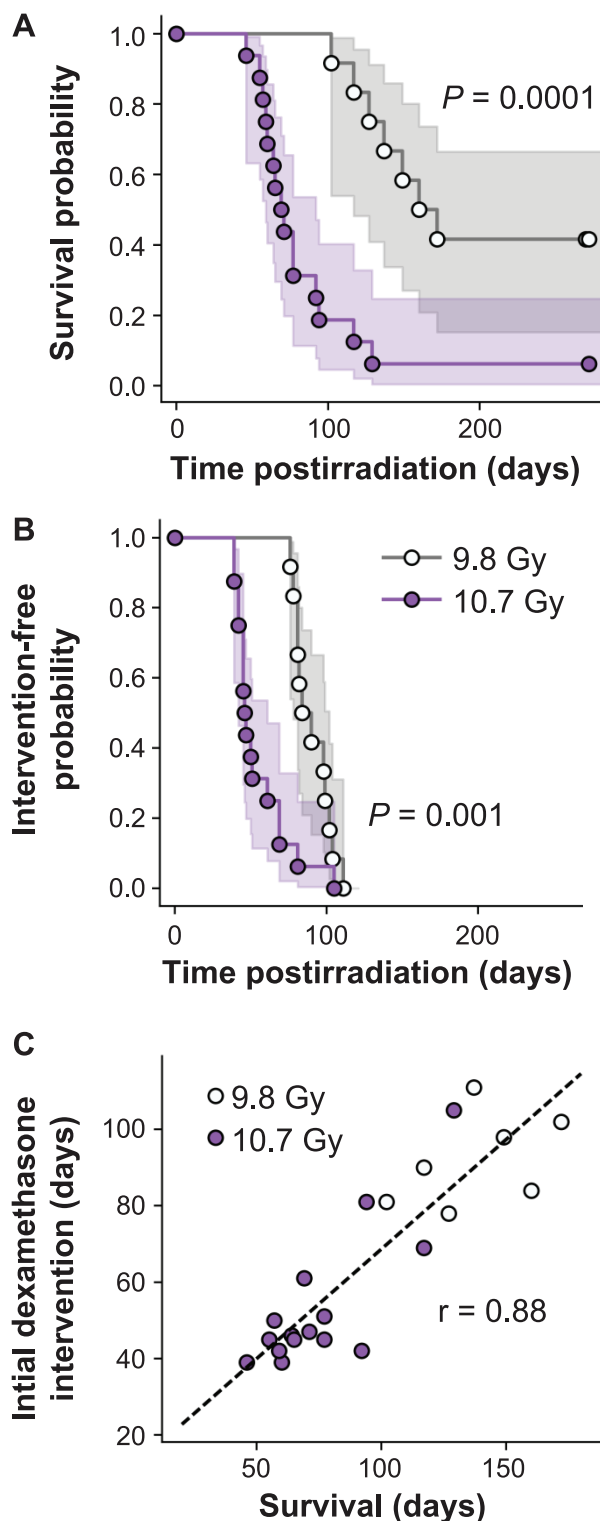


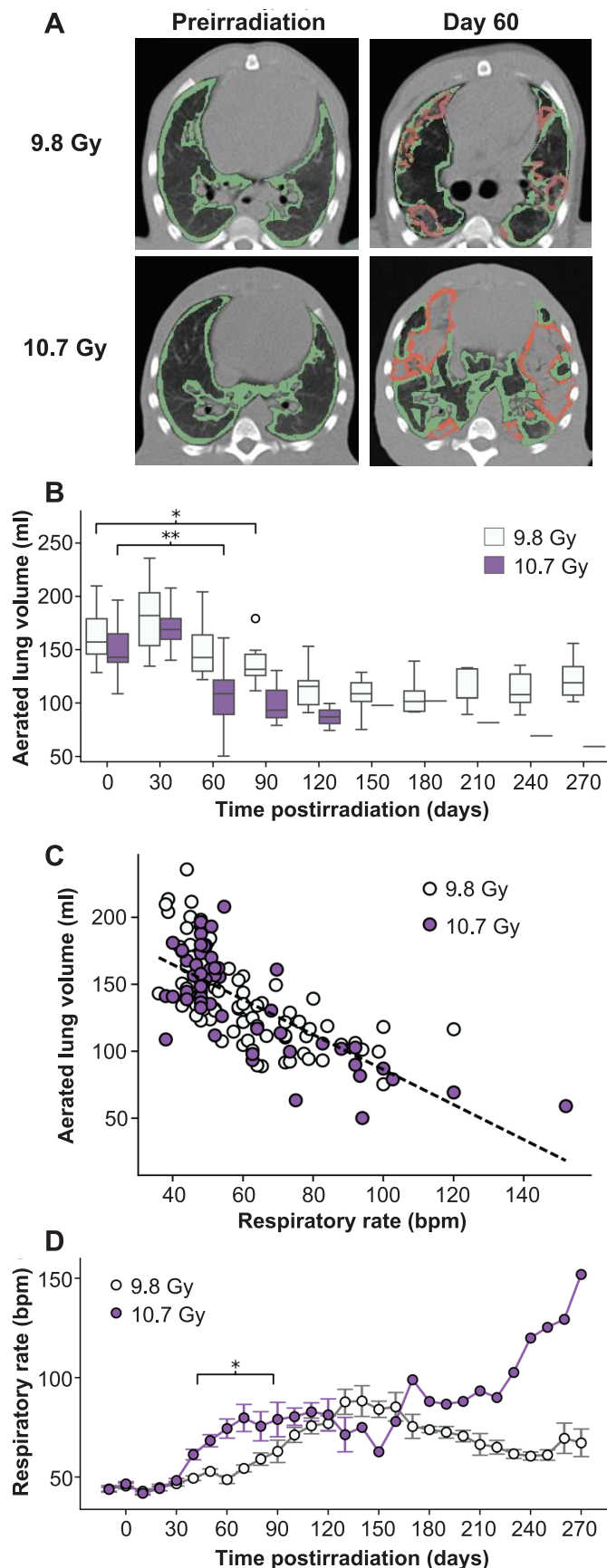
FIG. 2. Survival probability after WTLI. Panel A: Approximately 58% of 9.8 Gy WTLI animals (7 out of 12) and 94% of 10.7 Gy WTLI animals (15 of 16) died due to late radiation injury. The difference in survival rates between animals that received 9.8 or 10.7 Gy WTLI were statistically significant (log-rank $P = 0.0001$). Panel B: Similarly, event-free survival, using the date of the first dexamethasone intervention as a proxy for clinical pneumonitis, of 10.7 Gy WTLI NHPs was significantly reduced (log-rank $P = 0.001$) compared to 9.8 Gy WTLI animals. All animals received at least one dexamethasone treatment. Panel C: For all animals, the time to first dexamethasone treatment correlated strongly with survival (coefficient of correlation = 0.88).

time points. Strong differential expression was observed for the first 24 days after WTLI, which slowly reduced from month 1 to 3 (Fig. 5).

To identify differentially expressed miRNA that may play a role in survival, we grouped animals into two cohorts, based on the expression of a given miRNA at a given time point (day 6 or 15) above or below the median abundance. miRNA with statistically significant differences (log-rank test $P < 0.05$) between the survival curves were examined. Using this miRNA abundance threshold, several sequences were identified that correlated with early death (<175 days) (Fig. 6A). For example, animals that expressed miR-26b-5p or -496 above the median abundance at day 6 after WTLI had reduced survival and 100% death before 175 days compared to animals that expressed those miRNAs at or below the median abundance (log-rank $P = 0.003$ and 0.025, respectively). Similarly, expression at or below the median abundance at day 6 of miR-33a-5p and -199a-3p was also associated with reduced survival and 100% death before 175 days. At day 15, expression of miR-496, -181a-5p, -185-5p, -191-3p, -200c-3p, -301a-5p, -340-3p and -433-3p above the median abundance and miR-29c-3p, -206 and -320d at or below the median abundance was associated with reduced survival (log-rank $P < 0.05$) and 100% death before day 175.

We also identified other miRNAs with statistically significant differences in survival of cohorts of animals that expressed a given miRNA above or below the median abundance, but where neither cohort experienced 100% death before the study end point (Fig. 6B). For example, expression above the median abundance of let-7g-5p, miR-28-3p, -32-5p, -197-3p, 301a-3p, -376a-3p and -1271-5p or expression at or below the median abundance of miR-15b-3p, -17-3p, -25-3p and -378i at 15 days after WTLI showed reduced survival (log-rank $P < 0.05$).

These survival profiles suggest that certain groups of miRNAs may be associated with different pathological mechanisms leading to radiation-induced death before the onset of symptoms. We identified the KEGG pathways associated with miR-26b-5p, -33a-5p, 199a-3p and -496 (associated with reduced survival and early death based on day 6 expression levels), miR-496, -29c-3p, 181a-5p, 185-5p, -191-3p, -200c-3p, -206, -301a-5p, -320d, -340-3p and -433-3p (associated with reduced survival and early death based on day 15 expression levels), and let-7g-5p, miR-15b-3p, -17-3p, -25-3p, -28-3p, -32-5p, -197-3p, -301a-3p, -376a-3p, -378i and -1271-5p (associated with reduced survival but not early death *per se* based on day 15 expression levels) (48). We found the miRNAs associated with early death at both day 6 and 15 interacted with genes involved in p53 signaling (Fig. 7A), whereas miRNAs that were associated with reduced survival, but not early death, interacted with genes involved in TGF- β /SMAD signaling (Fig. 7B). While different miRNAs were associated with early death based on day 6 and 15 abundance levels, both sets of miRNAs interacted with the same genes, including



the highly conserved cyclin family members (CCNE1, CCNB1, CCND1 and CCND2), CDK kinases (CDK2 and CDK6), and caspase family members (CASP8 and CASP9). These genes regulate essential cellular processes including cell cycle progression and apoptosis.

The miRNAs associated with reduced survival, but not early death, interact with TGF- β (TGFB2), its cell-surface receptor (TGFB1, TGFB2), SMAD family members (SMAD2, SMAD3, SMAD4, SMAD5, SMAD7), the SMAD-regulating SMURF family members (SMURF1, SMURF2), and BMP family members (BMP2, BMP4, BMP6, BMP7). These genes have been linked to the initiation and progression of fibrosis.

DISCUSSION

The radiation hematologic toxicity outcomes observed here are consistent with previously published findings in WTLI and PBI/BM5 models in NHPs (1, 51) and mice (40). Decrease in blood cells after partial-body irradiation is generally due to radiation-induced cell death as the blood recirculates rapidly through the irradiated field. Without significant exposure to bone marrow, neutropenia was not observed within the first month of exposure, but instead a compensatory increase in neutrophil counts was seen approximately two months postirradiation. This corresponds to the expected pattern of radiation-induced pneumonitis, and the effect was larger in the animals that received a higher radiation dose and succumbed to pneumonitis. Evidence of neutrophil infiltration in the lungs was also observed histologically.

As expected, based on previously published NHP studies (41, 44), the radiation-induced lung injuries observed in this study show dose-dependent development of pneumonitis and pulmonary fibrosis after acute WTLI. We found that animals that received high-dose irradiation experienced more severe and early onset of radiation-induced pneumonitis followed by development of pulmonary fibrosis. Pneumonitis was evidenced by the increase in the non-sedated respiratory rate, more frequent and early administration of dexamethasone treatment, and decreased aerated lung volume on CT radiographs. Furthermore, we found

FIG. 3. WTLI resulted in reduced aerated lung volume and increased respiratory rates. Panel A: Representative CT scan radiographs at preirradiation time point and at day 60 after WTLI for the two dose cohorts. The red contour lines indicate boundary areas of lung injury (pneumonitis/fibrosis) using the HU range of -300 to $+80$. The green contour lines indicate areas of normal lung. Panel B: Aerated lung volume after WTLI was reduced for both dose cohorts, with 10.7 Gy WTLI animals presenting a statistically significant loss in aerated lung volume at day 60 (0.7-fold-change, $P = 0.0004$), compared to day 90 for 9.8 Gy WTLI animals (0.8-fold-change, $P = 0.009$). Panel C: Aerated lung volume correlated with the non-sedated respiratory rate (NSRR) at day 60 after WTLI (coefficient of correlation = -0.71). Panel D: Mean NSRR increased over time after WTLI for both dose cohorts, with statistically significant ($*P < 0.05$) differences between the cohorts between 40–90 days.

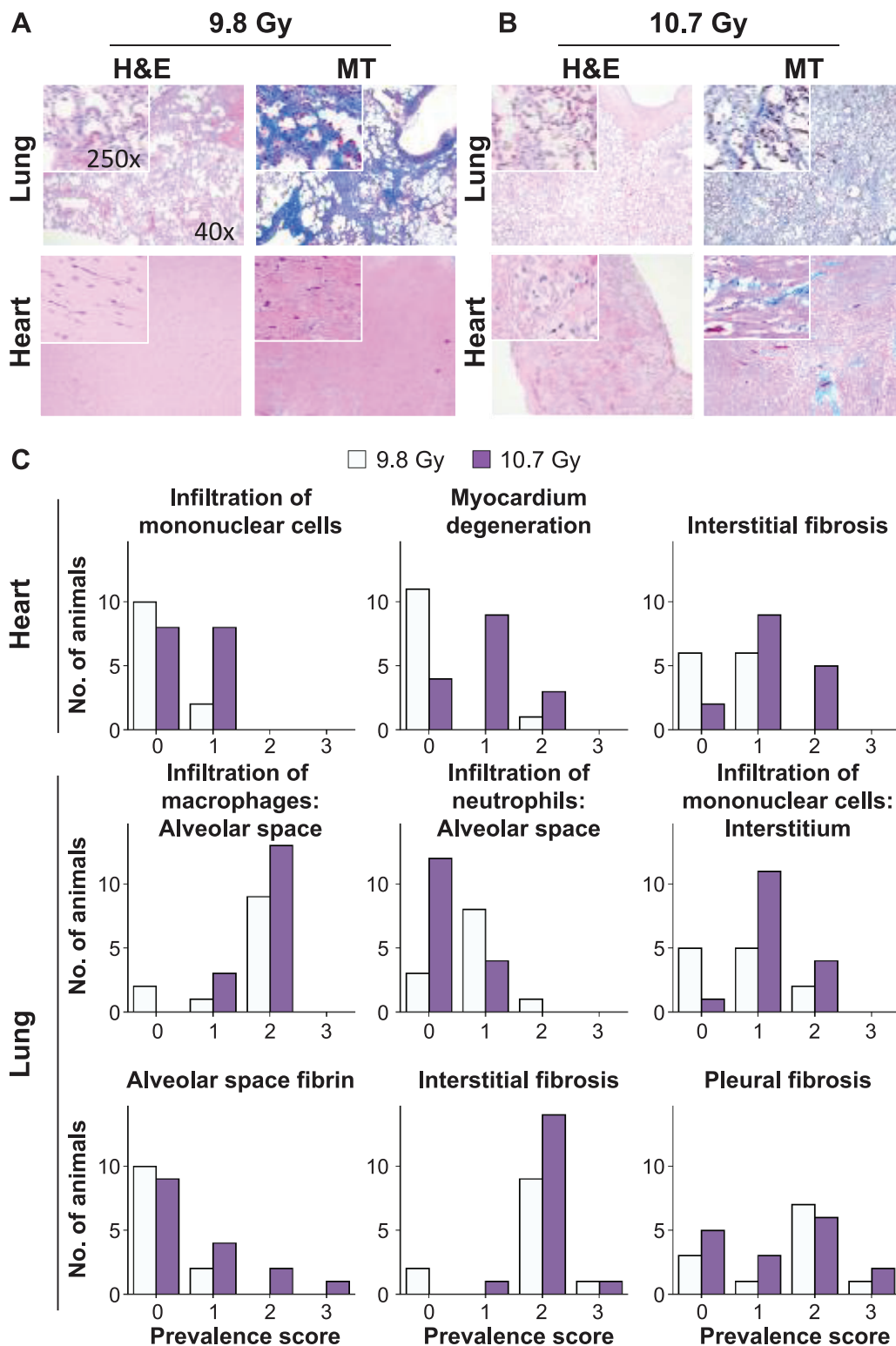


FIG. 4. Histopathology indicates significant pulmonary fibrosis in both dose cohorts. Panels A and B: H&E and MT staining of lung and heart tissue extracted after animal death. MT staining showed significant fibrosis in the lungs of both animals and in the heart tissue of 10.7 Gy WTLI animals. Panel C: Quantification of the prevalence of the indicated markers of heart and lung tissue from both dose cohorts, where 0 indicates that the marker was not present and 5 indicates that the marker was ubiquitous. In the heart, infiltration of mononuclear cells, myocardium degeneration and interstitial fibrosis were more prevalent in animals receiving 10.7 Gy WTLI ($P < 0.05$, Mann-Whitney U test). In the lung, statistical differences were observed between the prevalence distributions of the infiltration of neutrophils into the alveolar space and interstitial invasion of mononuclear cells ($P < 0.05$, Mann-Whitney U test).

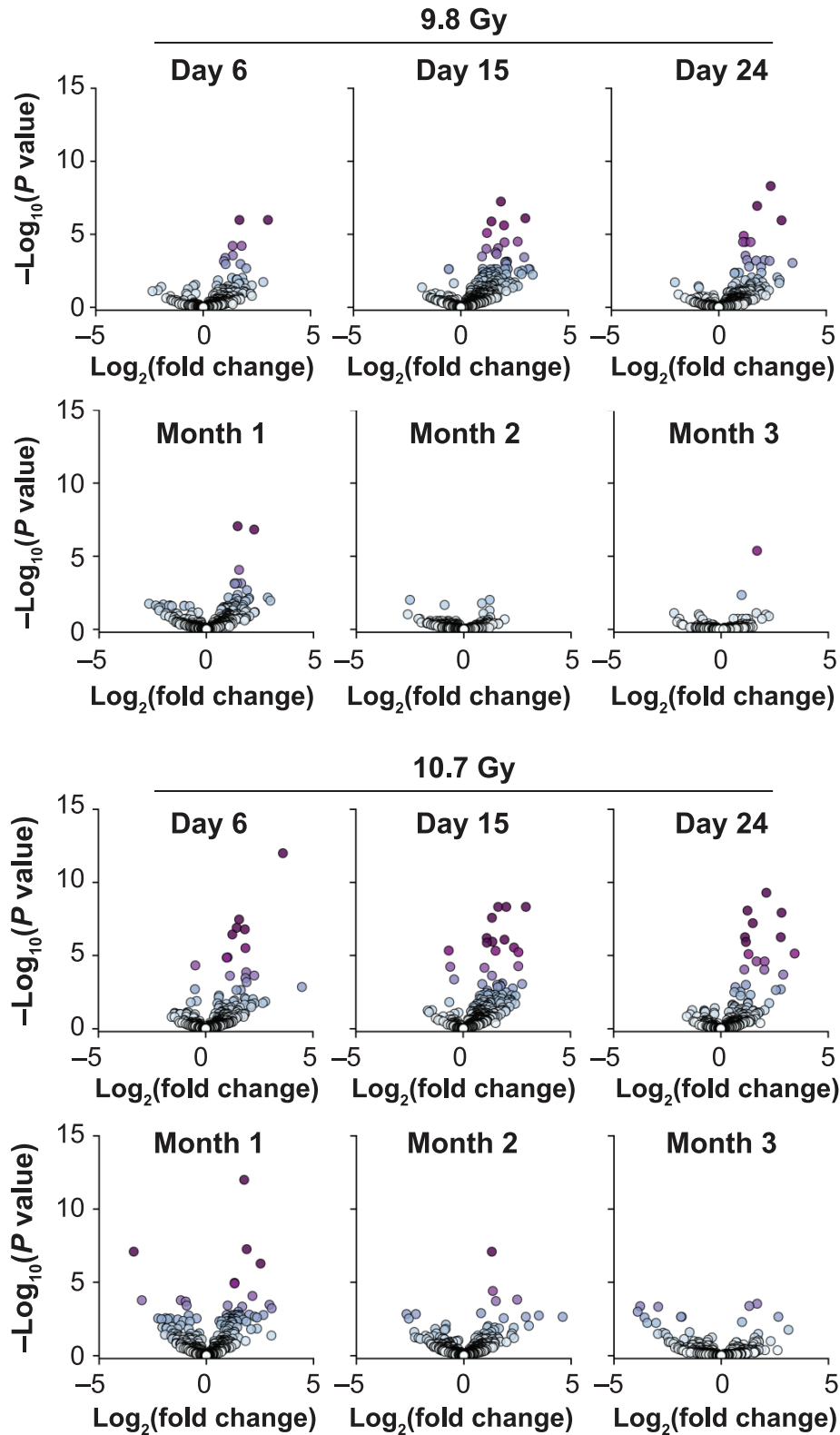


FIG. 5. WTLI induces major changes in the circulating miRNA profile. Volcano plots showing the \log_2 fold change versus $-\log_{10} P$ value for each circulating miRNA expressed above 5 RPM at the indicated time after WTLI for both dose cohorts. The expression of some miRNA in 9.8 Gy WTLI animals at 3 months, and 10.7 Gy WTLI animals and 2 and 3 months postirradiation may have been affected by dexamethasone treatment.

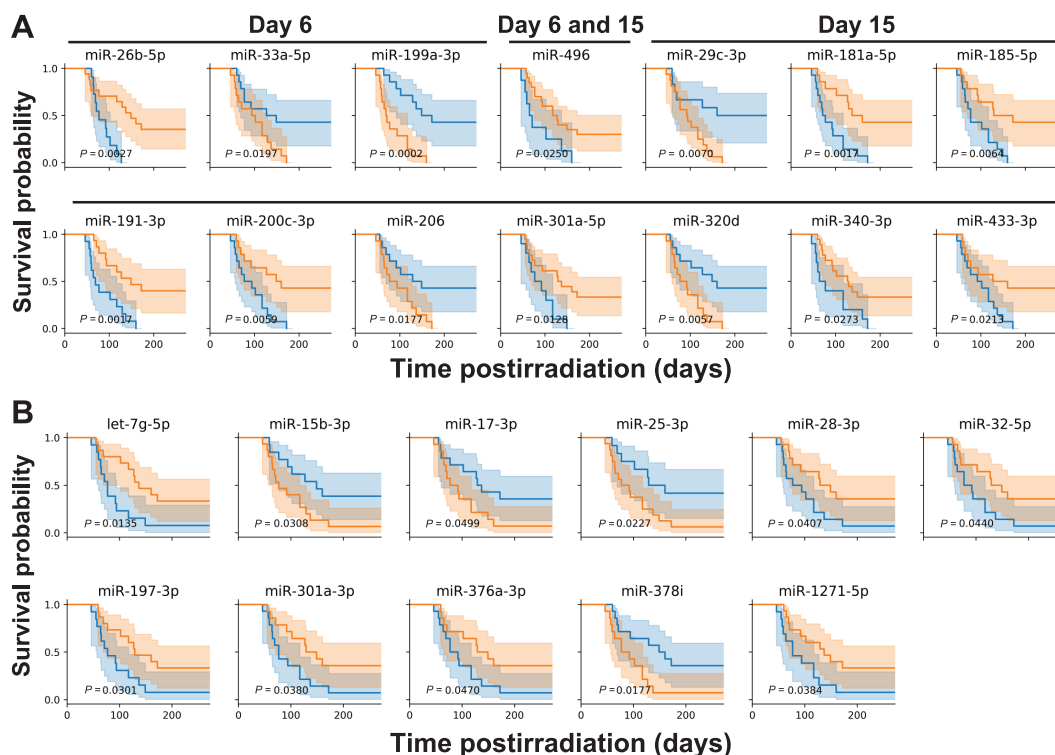


FIG. 6. The relative abundance of certain circulating miRNA was associated with reduced survival. For a given miRNA, NHPs were divided into two cohorts based on expression above (blue) or below (orange) the median abundance. For the indicated miRNA, the difference in survival between these two cohorts was statistically significant ($P < 0.05$, log-rank test), suggesting a role for these miRNAs as potential biomarkers for early identification of late organ injury after irradiation. Some miRNAs, based on the expression on day 6, day 6 and 15, or day 15, were associated with early death (100% death in one cohort within < 175 days (panel A), and other miRNAs, based on the expression on day 15 after WTLI were associated with reduced survival, but not early death *per se* (panel B).

that animals with early mortality (<175 days postirradiation) experienced respiratory failure from pneumonitis while animals that survived past 175 days showed persistent lung injury on CT scan and substantial fibroplasia on end point lung histology sections consistent with pulmonary fibrosis. Because the study end point went beyond the 180 days that is frequently used (44, 52, 53), we were able to observe both the recovery of radiation-induced pneumonitis and the time course for the development of pulmonary fibrosis. Histopathological analysis of heart tissue in the irradiated animals showed evidence of cardiac injury, particularly in 10.7 Gy WTLI animals. However, clinical signs of heart injury, such as elevated heart rate or cardiac failure, were not observed during the study.

We examined the changes in the circulating miRNA expression in the first few weeks after acute irradiation to identify markers that could pre-symptomatically predict the onset of DEARE. Radiation-induced differential expression of circulating miRNA was consistent with the response observed in mice after WTLI, with expression affected in the earliest time points and continuing levels of dysregulation that begin to return to preirradiation levels one to two months after WTLI (40). Dexamethasone intervention may have affected miRNA expression at 3 months postirradia-

tion for 9.8 Gy WTLI animals and at 2 and 3 months postirradiation for 10.7 Gy WTLI animals. Several miRNAs, including miR-34a-5p, -100-5p, -106a-5p, -107, -369-3p and -431-5p, were differentially expressed in both species prior to dexamethasone intervention. Some of these markers, including upregulation of miR-34a-5p, and downregulation of miR-100-5p, were observed to change in similar directions after TBI in NHPs (22, 26). This suggests that there may be an evolutionarily conserved molecular response to radiation injury that manifests itself as a characteristic systemic miRNA signature. Many of the differentially expressed miRNAs are predicted to affect diverse cellular processes, including fatty acid metabolism, the cell cycle, transcriptional regulation, and growth factor- and cytokine-mediated signaling pathways, which are consistent with the well-documented biological response to radiation injury.

Many of the differentially expressed miRNAs exhibited similar changes in abundance independent of dose (Fig. 6B), despite the differences in survival and other phenotypic outcomes. To identify miRNAs associated with adverse outcomes, we compared survival for animals expressing certain miRNAs above or below the median abundance at 6 or 15 days after WTLI. We identified a number of miRNAs

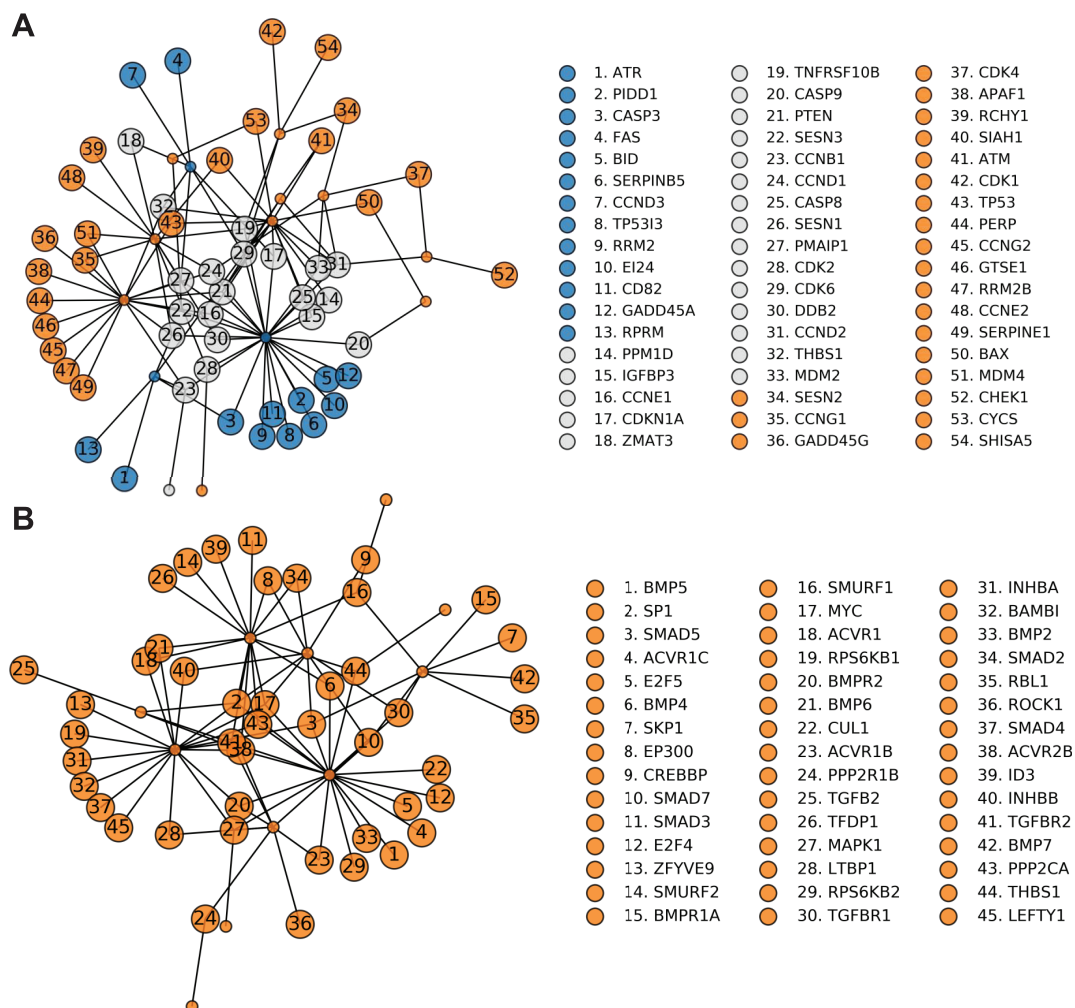


FIG. 7. Circulating miRNAs that correlate with reduced survival are associated with p53 and TGF- β signaling. Panel A: The circulating miRNA associated with reduced survival and 100% death before 175 days after WTLI are linked to p53 signaling genes. miRNA (small circles) have experimentally confirmed associations (Tarbase) with genes (large circles) in the p53 signaling pathway (65). Panel B: Circulating miRNAs associated with reduced survival, but not early death *per se*, are linked to genes in the TGF- β /SMAD signaling pathway. miRNA/genes are colored based on the time point they were observed/implicated (blue = only on day 6, orange = only on day 15, white = on both day 6 and 15).

that not only appeared to be associated with a statistically significant difference in survival, but also seem to predict early death (Fig. 6A). The fact that these miRNAs are associated with p53 signaling (Fig. 7A) is consistent with findings in humans that dysregulation of p53 signaling due to P53 and ATM polymorphisms is associated with radiation-induced pneumonitis in lung cancer patients treated with radiotherapy (54). The role of p53 signaling in the destruction of lung tissue in response to immune or oxidative stress has been established in the context of other diseases (55–58), and is consistent with the radiation-induced lung damage observed in this study.

Another set of miRNAs was identified that appeared to be associated with statistically significant differences in survival, but not early death (<175 days) *per se*, and are functionally linked to TGF- β /SMAD signaling. For example, our findings suggest that reduced expression of miR-

25-5p was associated with early death. This is consistent with previously published studies in mice and cell lines, which showed that decreased miR-25-5p production was associated with an increase in pro-fibrotic markers (e.g., collagen) and processes (e.g., epithelial-to-mesenchymal transition), and increased miR-25-5p production had the opposite effect (59–62). Since dysregulation of TGF- β /SMAD signaling is known to play a major role in the development and progression of fibrosis (63, 64), observed in most of the irradiated animals that did not succumb to pneumonitis, our findings suggest it may be possible to predict outcomes of WTLI pre-symptomatically using the day 15 circulating miRNA profile. Collectively, these results suggest that: 1. Changes in systemic miRNA expression within the first two weeks after WTLI can be used to asymptotically predict negative health outcomes that do not begin to manifest until months later; 2. The

initial transient differences in the circulating miRNA profile after radiation injury potentially have functional consequences for the animal; and 3. Analysis of the circulating miRNA profile may provide the ability to distinguish lethal pneumonitis from fibrosis.

SUPPLEMENTARY INFORMATION

Table S1. Supporting information detailing gender differences in survival, initial dexamethasone administration, and changes in aerated lung volume after WTLI.

ACKNOWLEDGMENTS

This project has been funded by the National Institute of Allergy and Infectious Disease (contract no. HHSN272201700012C and grant no. 2R44AI108019-04). ChromoLogic LLC staff adheres strictly to Ethical Scientific Conduct guidelines documented by the company in their Employee Agreement and all workers adhere to guidelines established by the National Institutes of Health. We thank James Axtelle and Michelle Nguyen for administrative assistance, J. Mark Cline, Thomas Register and Subhrajit Saha for helpful discussions, and the staff at Altascience for care of the animals.

Received: January 31, 2020; accepted: March 19, 2021; published online: April 15, 2021

REFERENCES

- MacVittie TJ, Bennett A, Booth C, Garofalo M, Tudor G, Ward A, et al. The prolonged gastrointestinal syndrome in rhesus macaques: the relationship between gastrointestinal, hematopoietic, and delayed multi-organ sequelae following acute, potentially lethal, partial-body irradiation. *Health Phys* 2012; 103:427–53.
- Buddemeier BR. Nuclear detonation fallout: Key considerations for internal exposure and population monitoring. Washington, DC: U.S. Department of Energy Office of Scientific and Technical Information 2018. (<https://www.osti.gov/biblio/1460062>)
- Duhachek-Muggy S, Bhat K, Medina P, Cheng F, He L, Alli C, et al. Radiation mitigation of the intestinal acute radiation injury in mice by 1-[(4-nitrophenyl)sulfonyl]-4-phenylpiperazine. *Stem Cells Trans Med* 2020; 9:106–19.
- Micewicz ED, Kim K, Iwamoto KS, Ratikan JA, Cheng G, Boxx GM, et al. 4-(Nitrophenylsulfonyl)piperazines mitigate radiation damage to multiple tissues. *PLoS One* 2017; 12: e0181577.
- Steinman J, Epperly M, Hou W, Willis J, Wang H, Fisher R, et al. Improved total-body irradiation survival by delivery of two radiation mitigators that target distinct cell death pathways. *Radiat Res* 2017; 189:68.
- Wei L, Leibowitz BJ, Epperly M, Bi C, Li A, Steinman J, et al. The GS-nitroxide JP4-039 improves intestinal barrier and stem cell recovery in irradiated mice. *Sci Rep* 2018; 8:2072.
- Yahyapour R, Amini P, Rezapoor S, Rezaeyan A, Farhood B, Cheki M, et al. Targeting of inflammation for radiation protection and mitigation. *Curr Mol Pharmacol* 2018; 11:203–10.
- Yahyapour R, Shabeeb D, Cheki M, Musa AE, Farhood B, Rezaeyan A, et al. Radiation protection and mitigation by natural antioxidants and flavonoids: implications to radiotherapy and radiation disasters. *Curr Mol Pharmacol* 2018; 11:285–304.
- Chiang C, Liu W, Jung S, Chen F, Wu C, McBride W, et al. Compartmental responses after thoracic irradiation of mice: strain differences. *Int J Radiat Oncol Biol Phys* 2005; 62:862–71.
- Liu K, Singer E, Cohn W, Micewicz E, McBride W, Whitelegge J, et al. Time-dependent measurement of nrf2-regulated antioxidant response to ionizing radiation toward identifying potential protein biomarkers for acute radiation injury. *Proteomics Clin Appl* 2019; 13:e1900035.
- Marchetti F, Coleman MA, Jones IM, Wyrobek AJ. Candidate protein biosimeters of human exposure to ionizing radiation. *Int J Radiat Biol* 2006; 82:605–39.
- Lee Y, Pujol Canadell M, Shuryak I, Perrier JR, Taveras M, Patel P, et al. Candidate protein markers for radiation biodosimetry in the hematopoietically humanized mouse model. *Sci Rep* 2018; 8:1–11.
- Johnston C, Wright T, Rubin P, Finkelstein J. Alterations in the expression of chemokine mRNA levels in fibrosis-resistant and -sensitive mice after thoracic irradiation. *Exp Lung Res* 1998; 24:321–37.
- Johnston C, Piedboeuf B, Baggs R, Rubin P, Finkelstein J. Differences in correlation of mRNA gene expression in mice sensitive and resistant to radiation-induced pulmonary fibrosis. *Radiat Res* 1995; 142:197–203.
- Purbey P, Scumpia P, Kim P, Tong A, Iwamoto K, McBride W, et al. Defined sensing mechanisms and signaling pathways contribute to the global inflammatory gene expression output elicited by ionizing radiation. *Immunity* 2017; 47:421–34.
- Li S, Lu X, Feng J Bin, Tian M, Liu QJ. Identification and validation of candidate radiation-responsive genes for human biodosimetry. *Biomed Environ Sci* 2017; 30:834–40.
- Dodge A, Brunet E, Chen S, Goulpeau J, Labas V, Vinh J, et al. PDMS-based microfluidics for proteomic analysis. *Analyst* 2006; 131:1122–8.
- Brzoska K, Kruszewski M. Toward the development of transcriptional biodosimetry for the identification of irradiated individuals and assessment of absorbed radiation dose. *Radiat Env Biophys* 2015; 54:353–63.
- Aryankalayil MJ, Chopra S, Levin J, Eke I, Makinde A, Das S, et al. Radiation-induced long noncoding rnas in a mouse model after whole-body irradiation. *Radiat Res* 2018; 189:251.
- Ostheim P, Haupt J, Herodin F, Valente M, Drouet M, Majewski M, et al. MiRNA expression patterns differ by total- or partial-body radiation exposure in baboons. *Radiat Res* 2019; 192:579–88.
- Jacob NK, Cooley J V., Yee TN, Jacob J, Alder H, Wickramasinghe P, et al. Identification of sensitive serum microRNA biomarkers for radiation biodosimetry. *PLoS One* 2013; 8:e57603.
- Menon N, Rogers CJ, Lukaszewicz AI, Axtelle J, Yadav M, Song F, et al. Detection of acute radiation sickness: a feasibility study in non-human primates circulating miRNAs for triage in radiological events. *PLoS One* 2016; 11:e0167333.
- Dinh TKT, Fendler W, Chalubinska-Fendler J, Acharya SS, O'Leary C, Deraska PV, et al. Circulating miR-29a and miR-150 correlate with delivered dose during thoracic radiation therapy for non-small cell lung cancer. *Radiat Oncol* 2016; 11:1–11.
- Aryankalayil MJ, Chopra S, Makinde A, Eke I, Levin J, Shankavaram U, et al. Microarray analysis of miRNA expression profiles following whole body irradiation in a mouse model. *Biomarkers* 2018; 23:689–703.
- Fendler W, Madzio J, Kozinski K, Patel K, Janikiewicz J, Szopa M, et al. Differential regulation of serum microRNA expression by HNF1beta and HNF1alpha transcription factors. *Diabetologia* 2016; 59:1463–73.
- Fendler W, Malachowska B, Meghani K, Konstantinopoulos PA, Guha C, Singh VK, et al. Evolutionarily conserved serum microRNAs predict radiation-induced fatality in nonhuman primates. *Sci Transl Med* 2017; 9:eal2408.
- Gilad S, Meiri E, Yogeve Y, Benjamin S, Lebanony D, Yerushalmi N, et al. Serum microRNAs are promising novel biomarkers. *PLoS One* 2008; 3:1–7.
- Bartel DP. MicroRNAs: target recognition and regulatory functions. *Cell* 2009; 136:215–33.
- Valadi H, Ekstrom K, Bossios A, Sjostrand M, Lee JJ, Lotvall JO.

- Exosome-mediated transfer of mRNAs and microRNAs is a novel mechanism of genetic exchange between cells. *Nat Cell Biol* 2007; 9:654–9.
30. Li L, Lu M, Fan Y, Shui L, Xie S, Sheng R, et al. High-throughput and ultra-sensitive single-cell profiling of multiple microRNAs and identification of human cancer. *Chem Commun* 2019; 55:10404–7.
 31. Huang G, Sun J, Lu Y, Liu Y, Cao H, Zhang H, et al. MiR-200 family and cancer: From a meta-analysis view. *Mol Asp Med* 2019; 7:57–71.
 32. Landgraf P, Rusu M, Sheridan R, Sewer A, Iovino N, Aravin A, et al. A mammalian microRNA expression atlas based on small RNA library sequencing. *Cell* 2007; 129:1401–14.
 33. Ludwig N, Leidinger P, Becker K, Backes C, Fehlmann T, Pallasch C, et al. Distribution of miRNA expression across human tissues. *Nucleic Acids Res* 2016; 44:3865–77.
 34. Faruq O, Vecchione A. microRNA: Diagnostic perspective. *Front Med* 2015; 2:51.
 35. Neudecker V, Brodsky KS, Kreth S, Ginde AA, Eltzschig HK. Emerging roles for MicroRNAs in perioperative medicine. *Anesthesiology* 2016; 124:489–506.
 36. Wang J, Chen J, Sen S. MicroRNA as biomarkers and diagnostics. *J Cell Physiol* 2016; 231:25–30.
 37. Condrat CE, Thompson DC, Barbu MG, Bugnar OL, Boboc A, Cretoiu D, et al. miRNAs as Biomarkers in disease: Latest findings regarding their role in diagnosis and prognosis. *Cells* 2020; 9:276.
 38. McBride W, Vegesna V. Role of the thymus in radiation-induced lung damage after bone marrow transplantation. *Radiat Res* 1997; 147:501–5.
 39. Down J, Nicholas D, Steel G. Lung damage after hemithoracic irradiation: dependence on mouse strain. *Radiother Oncol* 1986; 6:43–50.
 40. Rogers CJ, Lukaszewicz AI, Yamada-Hanff J, Micewicz ED, Ratikan JA, Starbird MA, et al. Identification of miRNA signatures associated with radiation-induced late lung injury in mice. *PLoS One* 2020; 15:e0232411.
 41. Garofalo M, Bennett A, Farese AM, Ward A, Taylor-Howell C, Cui W, et al. The delayed pulmonary syndrome following acute high-dose irradiation: A rhesus macaque model. *Health Phys* 2014; 106:330.
 42. Farese AM, Cohen M V., Katz BP, Smith CP, Jackson W, Cohen DM, et al. A nonhuman primate model of the hematopoietic acute radiation syndrome plus medical management. *Health Phys* 2012; 103:367–82.
 43. De Faria EB, Barrow KR, Ruehle BT, Parker JT, Swartz E, Taylor-Howell C, et al. The evolving mcart multimodal imaging core: Establishing a protocol for computed tomography and echocardiography in the rhesus macaque to perform longitudinal analysis of radiation-induced organ injury. *Health Phys* 2015; 109:479–92.
 44. Thrall KD, Mahendra S, Jackson MK, Jackson W, Farese AM, MacVittie TJ. A comparative dose-response relationship between sexes for mortality and morbidity of radiation-induced lung injury in the rhesus macaque. *Health Phys* 2019; 116:354–65.
 45. Parker GA, Li N, Takayama K, Farese AM, MacVittie TJ. Lung and heart injury in a nonhuman primate model of partial-body irradiation with minimal bone marrow sparing: Histopathological evidence of lung and heart injury. *Health Phys* 2019; 116:383–400.
 46. Kirschner MB, Kao SC, Edelman JJ, Armstrong NJ, Vallely MP, van Zandwijk N, et al. Haemolysis during sample preparation alters microRNA content of plasma. *PLoS One* 2011; 6:e24145.
 47. Law CW, Chen Y, Shi W, Smyth GK. Voom: Precision weights unlock linear model analysis tools for RNA-seq read counts. *Genome Biol* 2014; 15:1–17.
 48. Vlachos IS, Zagganas K, Paraskevopoulou MD, Georgakilas G, Karagkouni D, Vergoulis T, et al. DIANA-miRPath v3.0: deciphering microRNA function with experimental support. *Nucleic Acids Res* 2015; 43:W460–6.
 49. Mantel N. Evaluation of survival data and two new rank order statistics arising in its consideration. *Cancer Chemother Rep* 1966; 50:163–70.
 50. Greenwood MJ. The natural duration of cancer. In: Reports on public health and medical subjects. London: HMSO; 1926. p. 1–26.
 51. Ghandhi SA, Turner HC, Shuryak I, Dugan GO, Daniel Bourland J, Olson JD, et al. Whole thorax irradiation of non-human primates induces persistent nuclear damage and gene expression changes in peripheral blood cells. *PLoS One* 2018; 13:1–24.
 52. MacVittie TJ, Farese AM, Parker GA, Jackson W. The time course of radiation-induced lung injury in a nonhuman primate model of partial-body irradiation with minimal bone marrow sparing: Clinical and radiographic evidence and the effect of neupogen administration. *Health Phys* 2019; 116:366–82.
 53. MacVittie TJ, Gibbs A, Farese AM, Barrow K, Bennett A, Taylor-Howell C, et al. AEOL 10150 mitigates radiation-induced lung injury in the nonhuman primate: Morbidity and mortality are administration schedule-dependent. *Radiat Res* 2017; 187:298–318.
 54. Yang M, Zhang L, Bi N, Ji W, Tan W, Zhao L, et al. Association of P53 and ATM polymorphisms with risk of radiation-induced pneumonitis in lung cancer patients treated with radiotherapy. *Int J Radiat Oncol Biol Phys* 2011; 79:1402–7.
 55. Sagiv A, Bar-Shai A, Levi N, Hatzav M, Zada L, Ovadya Y, et al. p53 in bronchial club cells facilitates chronic lung inflammation by promoting senescence. *Cell Rep* 2018; 22:3468–79.
 56. Shenberger JS, Dixon PS. Oxygen induces S-phase growth arrest and increases p53 and p21(WAF1/CIP1) expression in human bronchial smooth-muscle cells. *Am J Respir Cell Mol Biol* 1999; 21:395–402.
 57. Bian T, Gibbs JD, Orvell C, Imani F. Respiratory syncytial virus matrix protein induces lung epithelial cell cycle arrest through a p53 dependent pathway. *PLoS One* 2012; 7:e38052.
 58. Damico R, Simms T, Kim BS, Tekeste Z, Amankwan H, Damarla M, et al. p53 mediates cigarette smoke-induced apoptosis of pulmonary endothelial cells: inhibitory effects of macrophage migration inhibitor factor. *Am J Respir Cell Mol Biol* 2011; 44:323–32.
 59. Tang Q, Zhong H, Xie F, Xie J, Chen H, Yao G. Expression of miR-106b-25 induced by salvianolic acid B inhibits epithelial-to-mesenchymal transition in HK-2 cells. *Eur J Pharmacol* 2014; 741:97–103.
 60. Dirx E, Gladka MM, Philippen LE, Armand A-S, Kinet V, Leptidis S, et al. Nfat and miR-25 cooperate to reactivate the transcription factor Hand2 in heart failure. *Nat Cell Biol* 2013; 15:1282–93.
 61. Divakaran V, Adroge J, Ishiyama M, Entman ML, Haudek S, Sivasubramanian N, et al. Adaptive and maladaptive effects of SMAD3 signaling in the adult heart after hemodynamic pressure overloading. *Circ Heart Fail* 2009; 2:633–42.
 62. Sarkozy M, Kahan Z, Csont T. A myriad of roles of miR-25 in health and disease. *Oncotarget* 2018; 9:21580–612.
 63. Meng X-M, Nikolic-Paterson DJ, Lan HY. TGF-beta: the master regulator of fibrosis. *Nat Rev Nephrol* 2016; 12:325–38.
 64. Biernacka A, Dobaczewski M, Frangogiannis NG. TGF-beta signaling in fibrosis. *Growth Factors* 2011; 29:196–202.
 65. Karagkouni D, Paraskevopoulou MD, Chatzopoulos S, Vlachos IS, Tastsoglou S, Kanellos I, et al. DIANA-TarBase v8: a decade-long collection of experimentally supported miRNA-gene interactions. *Nucleic Acids Res* 2018; 46:D239–45.